Effects of multiple insufficient charging and discharging on compressed carbon dioxide energy storage

D. L. Yang [a,b], G. H. Tang [a,**] Q. Sheng [c], X. L. Li [a], Y. H. Fan [a], Y. L. He [a], K. H. Luo [b, *, **]

[a] MOE Key Laboratory of Thermo-Fluid Science and Engineering, School of Energy and Power Engineering, Xi'an Jiaotong University, Xi'an 710049, China

[b] Department of Mechanical Engineering, University College London, London WC1E 7JE, United Kingdom

[c] School of Science and Technology, City University of London, London EC1V 0HB, United Kingdom

[a, **] Corresponding author. Tel: +86(0)29-82665319 E-mail: ghtang@mail.xjtu.edu.cn

[b, *, **] Corresponding author. Tel: +44(0)20-76793916 E-mail: k.luo@ucl.ac.uk

* Corresponding author ** The two authors have the same contribution to this study.

Abstract

Compressed carbon dioxide is a promising energy storage technology. However, renewable energy variability can lead to insufficiency during charging and discharging. The present work systematically investigates the effect of charging/discharging insufficiency on compressed carbon dioxide energy storage systems from the viewpoint of transient thermodynamic cycles. The insufficiency extent is defined based on the pressure at the high-pressure tank when disturbances occur. Then the effects of insufficiency extent are investigated in three typical scenarios. In the results, the effects of charging/discharging insufficiency on the efficiency, storage density and power output of the energy storage system during long-term operation are demonstrated. The efficiency of the system during the whole working period is 57.78%, lower than the design efficiency of 59.66%. In particular, the energy storage density is reduced dramatically to 197.60 kJ·m^{-3}, which is 78.2% of the storage density of 252.68 kJ·m^{-3} at design conditions. Besides, the average output power of the turbine is reduced to 95.70% of the design value. The present work provides an improved understanding of the charging and discharging for compressed carbon dioxide energy storage, especially when renewables are integrated.

Keywords: Charging and discharging; renewable energy variability; compressed carbon dioxide energy storage; dynamic operation analysis

Nomenclature

E	exergy, kW	*Subscripts*	
h	specific enthalpy, $kJ \cdot kg^{-1}$	a	ambient
$\dot{m}$	mass flow rate, $kg \cdot s^{-1}$	D	design condition
n	number	Des	exergy destruction
P	pressure, MPa	D, max	the maximum value of the design condition
p	pressure for disturbance, MPa	D, min	the minimum value of the design condition
$\dot{q}$	heat rate, $kJ \cdot s^{-1}$	E	energy storage
Q	heat capacity, kJ	ex	exergy
s	specific entropy, $kJ \cdot kg^{-1} \cdot K^{-1}$	F	fuel exergy
t	time, s	i	each component
T	temperature, ℃	ini	initial
u	specific internal energy, $kJ \cdot kg^{-1}$	P	product exergy
V	storage volume, m^3	rt	round-trip
$\dot{w}$	power, kW	s	isentropic process
W	total power, kWh		
$\overline{W}$	average power, kW	*Abbreviations*	
		C	compressor
Greek letters		HPT	high-pressure storage tank
ρ	density, $kg \cdot m^{-3}$	LPT	low-pressure storage tank
η	efficiency	T	turbine
		TES	thermal energy storage

1. Introduction

Compressed carbon dioxide energy storage (CCES) technology is drawing more and more attention because of its advantages in the favourable thermo-physical properties of carbon dioxide (CO_2), eco-friendliness, safety and ability to integrate renewable energy for the ultimate decarbonization of power systems [1]. It can be used to store not only the excessive electricity in normal electricity grids but also the electricity generated from renewable energy like other compressed fluid energy storage systems [2-6].

Energy storage systems are normally described as “Peak Shaving and Valley Filling”. However, this does not mean that the output of the energy storage system can avoid any fluctuation. Unlike fossil-power plants, renewables-based electricity generators bring significant uncertainty to the energy storage system. When they are integrated into a compressed CO_2 energy storage system, it is necessary to investigate their operations subject to the variability of renewable energy.

Renewable energy has been extensively integrated into CO_2-based energy storage and generation systems in engineering [7-12]. For example, solar energy has been integrated into the CO_2-based energy generation or storage systems in the Sunshot Initiative project [7, 8], the Supercritical Transformational Electric Power project (STEP) [9, 10] in the US, the SOLARSCO_2OL project in the EU [11], and a 10 MW Supercritical CO_2 power system in China [12].

As seen above, it is reasonable to believe that the variability of renewables (e.g., solar energy) has been considered in some of the industrial projects above. Even some CCES projects (the Energy Dome Project in Italy [13], a CCES system embedded with a flywheel energy storage feature in China [14]) based on traditional energy sources, may suffer from some variability in energy input, due to the natural fluctuation of the excess electricity in normal electricity grids. Therefore, relevant issues should be investigated in academia carefully, as shown below.

In academia, many different aspects of the compressed CO_2 energy storage system have been investigated. The studies are mainly focused on the performance analysis under steady state. Wang et al. [15] presented a novel energy storage system based on liquid carbon dioxide, which has high energy density compared with advanced adiabatic compressed air energy storage (AA-CAES) and a round-trip

efficiency of 56.64% is achieved. Zhang et al. [16] found that the compressed CO_2 energy storage system has higher performance than both liquid CO_2 system and advanced adiabatic compressed air energy storage system. Liu et al. [17] presented that the supercritical CO_2 energy storage has a higher energy density than that of CAES. Zhang et al. [18] proposed and analyzed a compressed CO_2 energy storage system with hot water as the heat storage medium, which has high round-trip efficiency and energy density. As the compressed CO_2 energy storage technology is still under development, some existing CO_2 power generation and other relevant technologies can be used as references, such as energy storage and power generation with CO_2 [19-21], S-CO_2 coal-fired Brayton cycle [22-26], S-CO_2 Brayton cycle for solar energy [27], reviews for S-CO_2 power cycle [28, 29] and components level investigation [30-33]. Especially, Yang et al. [19] proposed a feasibility analysis for the integration and conversion of CO_2 power generation and energy storage, in which high efficiencies are achieved. Overall, the performance evaluations can pave the way for application of CO_2-based thermodynamic cycles but fail to reveal the effects of variability of energy input, which is essential not only as a dynamic question but also an off-design problem.

To describe such a transient problem at off-design conditions, firstly, solar energy will be taken to explain what the variability of renewables means for a CCES system. The solar energy intensity in three successive days in November 2020 is given in Fig. 1 from the Duren Tiga weather station at PLN Research Institute, Indonesia [34], and the charging/discharging curves are also schematically shown. No idle periods between the charging and discharging are assumed. The solid lines in blue and in yellow mean the charging and discharging curves of pressure in the high-pressure tank at design conditions (the extent of charging is indicated by the normalized pressure, which will be detailed later). They are sufficient for charging/discharging at design conditions. The dashed lines represent the actual charging curves. The accumulated solar energy each day denotes the energy input available for its energy storage system, where a noticeable variability can be observed. Sufficient charging/discharging only occurs on the second day, and the insufficiency extent on the first day and the third day could be about 75 and 50%, respectively. Here, the insufficiency extent of charging/discharging is evaluated by the normalized pressure at the high-pressure tank.

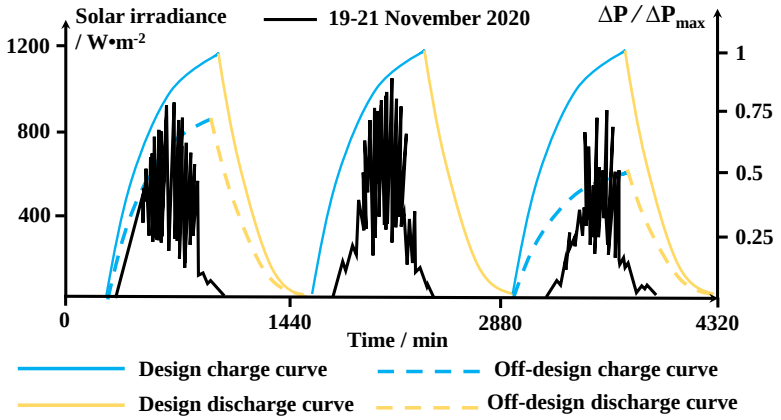

Fig. 1 The integration of the storage system and accessible renewable energy [34] with the schematic of insufficient charging and discharging at off-design conditions.

Relevant advances in dynamic modelling and off-design analysis are summarized below. For dynamic modelling, several investigations [35-37] can be found on the dynamical modelling of CCES systems, which are helpful for the proposed question. The system model based on the first and second laws of thermodynamics was established in [36], and experimental data were shown in [37]. And several papers [38-40] on the dynamics of compressed air energy storage systems are informative as well. On the off-design analysis, Wan et al. [41] investigated the effects of ambient temperature variables in a year on the performance of a concentrated solar power (CSP) driven supercritical power cycle. They proposed optimal operation parameters and control schemes under off-design conditions. They found that lower ambient temperature can save the total power output accounting for 1.02% of the yearly power output, while the higher temperature causes the total wasted power output accounting for 0.66%. Thanganadar et al. [42] also focused on the off-design analysis of a supercritical cycle for CSP application under variable ambient temperature, molten-salt temperature, and flow rate. The rest of the off-design investigations [43,44] are mainly focused on other cycles and also limited to certain specific parameters of components, including heat source mass flow rate, heat source temperature [43], heat sink temperature and mass flow rate ratio [44]. However, the issue of insufficiency in charging/discharging has not been analyzed carefully, which relates to the effect of the variability of renewable energy on the CCES system.

Thus, the first purpose of the present work is to propose and formulate a specific question, as shown in Sec. 2, where the question in Fig. 1 is further elaborated. In Sec. 3, the dynamic modelling of charging/discharging is introduced, and the method is validated by comparing it with available

experimental and simulation data. In Sec. 4, the energy storage efficiency and density of energy storage systems are evaluated for charging/discharging insufficiency. In Sec. 5, further impacts of the present work on tech-economic analysis are discussed. A conclusion is finally given in Sec. 6.

2 Problem Statement and Analysis method

To quantify the insufficiency of charging/discharging, a design condition of a CCES system is presented as a baseline, i.e., sufficient charging/discharging. Then a definition of insufficient charging/discharging is presented. The analysis method is proposed to tackle the issue.

2.1 A sufficient charging/discharging: design condition

The schematic of a CCES system is shown in Fig. 2, including five key components: a compressor (C), a turbine (T), a high-pressure tank (HPT) and a low-pressure tank (LPT), and a thermal energy storage (TES) device. The process in blue denotes charging while that in yellow is for discharging. The working principle for the CCES system is as below.

1) During charging, the input electricity drives the compressor to pressurize CO_2 in the LPT into the HPT for higher pressure. The electricity is converted to the internal energy of CO_2 and stored in the HPT.

2) When CO_2 passes through the TES device during the charging, the compression heat is stored in the TES device.

3) During discharging, CO_2 absorbs the thermal energy in the TES device for higher temperatures.

4) Then CO_2 expands in the turbine, which drives generators to produce electricity. The internal energy of CO_2 is converted to electricity.

The specific system shown below is set as the baseline to evaluate the effects of renewable energy variability. Its system parameters are set based on several cases available in [36], which defines the so-called “design conditions”, as shown in Tab. 1. For simplicity, “a charging at design/off-design conditions” is referred to as “a sufficient/insufficient charging” (and similar for “a discharging”). In a sufficient charging, CO_2 in the LPT is charged into the HPT, with the pressure at the LPT reduced from $P'_{D,\,max}$ to $P'_{D,\,min}$ and with that at the HPT increasing from $P_{D,\,min}$ to $P_{D,\,max}$. In a sufficient discharging,

CO_2 in the HPT returns to the LPT, with that at the HPT decreasing from $P_{D,\,max}$ to $P_{D,\,min}$, and with that at the LPT improved from $P'_{D,\,min}$ to $P'_{D,\,max}$. In addition, the total power input of the compressor (2352.93 kWh), the total power output of the turbine (1403.79 kWh), round-trip efficiency (59.66%) and the energy storage density (252.68 kJ·m^{-3}) at design conditions are for comparison with those of the off-design cases shown later. Note that these specific parameters of the system under the design condition would enable a quantitative analysis for the system. But general findings regarding system performance with insufficient charging/discharging is more important.

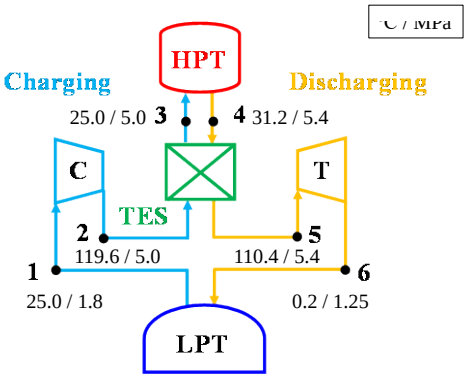

Fig. 2 The schematic of the compressed carbon dioxide energy storage system with parameters at the beginning of charging and discharging processes for the design condition.

Tab. 1 Parameters of the system under the design condition.

Components	Items	Symbols	Values
HPT	Volume (m^3)	V	10,000
	Initial temperature (℃)	T_{ini}	25
	Pressure range (MPa)	$P_{D,\,min}$- $P_{D,\,max}$	5.0-5.43
LPT	Volume (m^3)	V'	10,000
	Initial temperature (℃)	T'_{ini}	25
	Pressure range (MPa)	$P'_{D,\,max}$- $P'_{D,\,min}$	1.8-1.25
Other	CO_2 mass flow (kg/s)	m_{CO_2}	24
parameters	Ambient temperature (℃)	T_a	25
	Ambient pressure (MPa)	P_a	0.101
	Period (s)	t_D	3632
	Total power of compressor (kWh)	W_C	2352.93
	Total power of turbine (kWh)	W_T	1403.79

Round-trip efficiency	$\eta_{\mathrm{rt,\,D}}$	59.66%
Energy storage density (kJ·m^{-3})	ρ_{D}	252.68

2.2 Definition of insufficient charging/discharging: off-design conditions

Theoretically, charging can begin from any pressure and end at any higher pressure. Similarly, discharging can start from a certain pressure and end at a lower pressure. The parameters of successive charging and discharging can be understood as "a phase space of time, the pressure in charging, and the pressure in discharging", as indicated in Fig. 3(a). A clearly defined sufficient charging/discharging at design conditions is a point in the phase space (noted by the star in green), while the rest of the space can be referred to as "off-design conditions". For example, two dashed curves are given for off-design charging and discharging. It is observed that there can be a huge number of cases within off-design conditions. It is necessary to propose a method to extract the characteristics of insufficient charging/discharging to make a clear problem statement, otherwise, any further analysis of system performance is unachievable.

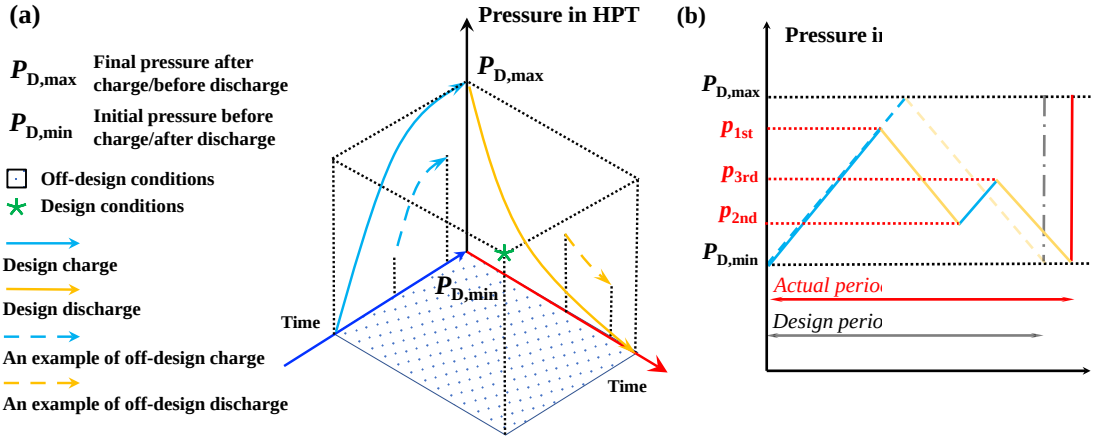

Fig. 3. (a) A schematic of the high complexity of off-design conditions: in the phase space of charging and discharging, the design condition is a point while the off-design condition can be anywhere in the rest of the space of the whole space except for the point. (b) The simplified question to investigate in the present work: modelling the charging/discharging insufficiency with three disturbances in the input or output of energy, indicated by p_{1st}, p_{2nd} and p_{3rd}.

In the present work, the insufficient charging/discharging processes are set up based on two

assumptions in terms of the pressure at the HPT: 1) the process begins with an uncharged HPT ($P = P_{D,\ min}$), while the final discharging ends with a sufficiently discharged HPT ($P = P_{D,\ min}$), and 2) the charging is assumed to be followed by the discharging, and the discharging is assumed to be followed by the charging. The extent of charging/discharging insufficiency is decided by the stoppings in charging or discharging. Then, the pressures at the HPT when a disturbance occurs are used to define the insufficiency extent.

Three successive stoppings are shown in Fig. 3(b) for a demonstration. The pressure increases from $P_{D,\ min}$ during a charging. The charging stops at p_{1st} before a full charging and turns to discharge for a certain period until the pressure at the HPT reaches a certain pressure at p_{2nd}. Then the HPT continues to be charged and its pressure increases to a certain pressure p_{3rd} and then turns to discharging again until the pressure returns to $P_{D,\ min}$. Also, the period of such an actual insufficient charging/discharging should differ from that of a designed condition as shown in Fig. 3(b).

2.3 Analysis method

As shown in Fig. 3(b), three disturbances are assumed above, and each of the disturbance extents is represented by a corresponding pressure (p_{1st}, p_{2nd} and p_{3rd}). Different extents of these disturbances can lead to complex situations of charging and discharging. Moreover, some limitations are applied to the values of p_{1st}, p_{2nd} and p_{3rd}, including $p_{1st} > p_{2nd}$ and $p_{2nd} < p_{3rd}$.

To perform quantitative evaluations of the disturbances above, the occupancy ratios in the high-pressure tanks are chosen to define the insufficiency extent. The pressure in the HPT is marked as p_x, which is expressed as:

$$p_x = P_{D,\ min} + x\left(P_{D,\ max} - P_{D,\ min}\right) \tag{1}$$

where x denotes the extent of charging/discharging. With $x = 0$, p_x denotes an uncharged HPT while $x = 1$ denotes a sufficiently charged one. Thus, $p_0 = P_{D,\ min}$, and $p_1 = P_{D,\ max}$. For example, $p_{0.5}$ means that the HPT is half charged, where the pressure at the HPT is in the average of “uncharged charged" and “sufficiently charged”. In the analysis below, the values of p_{1st}, p_{2nd} and p_{3rd} are expressed by p_x, where the values of x are chosen as 1, 0.75, 0.5, 0.25 and 0. For these chosen values, with a small x, p_x denotes a far insufficient charge due to an expected stopping while it means a deviation from “fully charged” for x approaching 1. Therefore, all the scenarios for insufficient charging and discharging can

be classified into four categories, which are charge begin, discharge end, charge midway and discharge midway as shown in Fig. 4. These processes will be rearranged in Sec. 4 for further analysis.

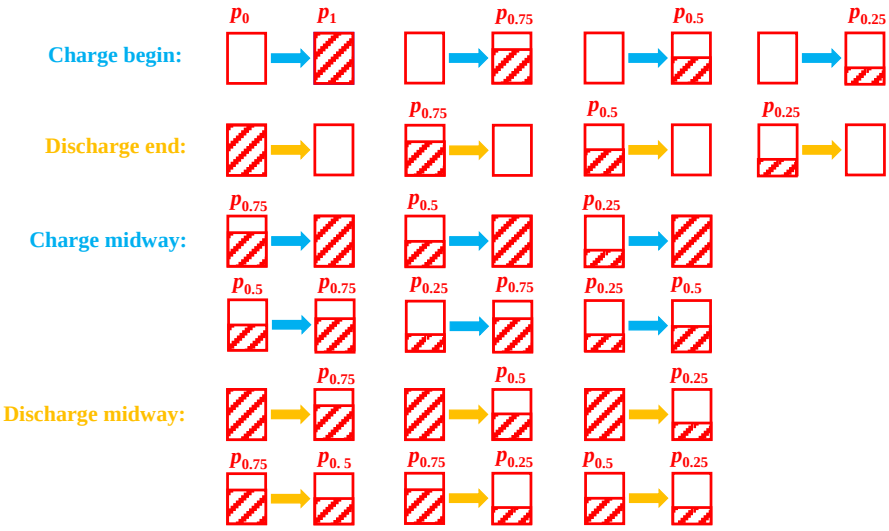

Fig. 4 Schematic of all the scenarios for insufficient charging and discharging with pressure changes in the high-pressure tank (HPT).

3. Thermodynamic modelling and validation

3.1 Performance evaluation criteria

The performance of a compressed CO_2 energy storage system can be evaluated from the viewpoints of energy and exergy. The former is interpreted by the round-trip efficiency and energy storage density. The latter is evaluated by exergy destruction and exergy efficiency of components, where exergy denotes the amount of work (= entropy-free energy) that a system can perform when it is brought into thermodynamic equilibrium with its environment.

The round-trip efficiency is defined as the ratio of the total power output to the total power consumption [36],

$$\eta_{rt} = \frac{W_T}{W_C} \tag{2}$$

The energy storage density is defined as the total power output per unit volume of storage [36],

$$\rho = \frac{W_T}{V} \tag{3}$$

where V is the sum of the volumes of the high-pressure and low-pressure storage tanks.

The exergy balance of the i_{th} component can be expressed as,

$$\dot{E}_{\mathrm{Des,i}}\left(t\right)=\dot{E}_{\mathrm{F,i}}\left(t\right)-\dot{E}_{\mathrm{P,i}}\left(t\right) \tag{4}$$

where $\dot{E}_{\mathrm{Des,i}}$, $\dot{E}_{\mathrm{F,i}}$ and $\dot{E}_{\mathrm{P,i}}$ represent the exergy destruction rate, the fuel exergy, and the product exergy rate in the i_{th} component, respectively.

The total exergy destruction of the i_{th} component is,

$$E_{\mathrm{Des,\,i}}=E_{\mathrm{F,\,i}}-E_{\mathrm{P,\,i}} \tag{5}$$

$$E_{\mathrm{F,\,i}}=\int_{process\ begin}^{process\ end}\dot{E}_{\mathrm{F,\,i}}\left(t\right)dt \tag{6}$$

$$E_{\mathrm{P,\,i}}=\int_{process\ begin}^{process\ end}\dot{E}_{\mathrm{P,\,i}}\left(t\right)dt \tag{7}$$

where $E_{\mathrm{F,\,i}}$ and $E_{\mathrm{P,\,i}}$ are the total fuel exergy and product exergy of the i_{th} component, respectively, and *process* in the equation refers to the charging and discharging corresponding to the operation of the i_{th} component.

The exergy efficiency of the i_{th} component is,

$$\eta_{\mathrm{ex,i}}=\frac{E_{\mathrm{P,i}}}{E_{\mathrm{F,i}}} \tag{8}$$

3.2 Thermodynamic modelling of charging/discharging

The system has main components including the compressor, turbine, high-pressure tank, low-pressure tank and thermal energy storage devices, as introduced in the following order. The following assumptions are made in the present model. 1) The mechanical kinetic energy and potential energy in the system are negligible. 2) Pressure drops, energy losses, heat and friction losses in pipes, valves and each component are negligible. 3) Mass flow rates are equal and stable during the round-trip process. 4) The power consumption of pumps in the system is neglected.

1) Compressor

The power consumption and total power consumption of the compressor are, respectively,

$$\dot{w}_{\mathrm{C}}\left(t\right)=\dot{m}_{\mathrm{char}}\left(t\right)\left(h_{2}\left(t\right)-h_{1}\left(t\right)\right) \tag{9}$$

$$W_{\mathrm{C}}=\int_{t_{\mathrm{begin\ char}}}^{t_{\mathrm{end\ char}}}\dot{w}_{\mathrm{C}}\left(t\right)dt \tag{10}$$

where $\dot{m}_{\mathrm{char}}$ is the mass flow rate during charging, and h_1 and h_2 are the real enthalpies of the inlet and outlet of the compressor, respectively. *t* stands for the time, and the subscripts *begin* and *end* indicate

the start and end of the process, respectively. The subscript *Char* stands for charging.

The real enthalpy can be calculated by the definition of the isentropic efficiency of the compressor,

$$\eta_{\mathrm{C}}(t)=\frac{h_{2,\mathrm{s}}(t)-h_1(t)}{h_2(t)-h_1(t)} \tag{11}$$

where $h_{2,\mathrm{s}}$ is the enthalpy during isentropic compression, which can be calculated by the equation of state,

$$h_{2,\mathrm{s}}(t)=f\left(s_{2,\mathrm{s}}(t),P_2(t)\right) \tag{12}$$

where P_2 is the outlet pressure of the compressor. The subscript "s" represents an isentropic compression process. The entropies of the inlet and outlet of the compressor are the same during the isentropic compression,

$$s_{2,\mathrm{s}}(t)=s_1(t) \tag{13}$$

The transient modelling requires the changing pressures at the compressor inlet and outlet. Thus, the isentropic efficiency of the compressor changes over time. The efficiency is related to the compression ratio, which is defined as the ratio of outlet to inlet pressure. An empirical formula in [36, 45] is adopted to describe how compression ratio affects the isentropic efficiency of the compressor,

$$\eta_{\mathrm{C}}(t)=1.0149-0.08534\left(\frac{P_2(t)}{P_1(t)}\right) \tag{14}$$

where P_1 and P_2 are the inlet and outlet pressures of the compressor, respectively.

2) Turbine

The power output and total power output of the turbine are, respectively,

$$\dot{w}_{\mathrm{T}}(t)=\dot{m}_{\mathrm{dischar}}(t)\left(h_5(t)-h_6(t)\right) \tag{15}$$

$$W_{\mathrm{T}}=\int_{t_{\text{begin dischar}}}^{t_{\text{end dischar}}}\dot{w}_{\mathrm{T}}(t)dt \tag{16}$$

where $\dot{m}_{\mathrm{dischar}}$ is the mass flow rate during the discharging, h_5 and h_6 are the real enthalpies of the inlet and outlet of the turbine, respectively, and $t_{\text{begin dischar}}$ and $t_{\text{end dischar}}$ are the beginning and end time of the discharging, respectively.

The real enthalpy can be calculated by the definition of the isentropic efficiency of the turbine,

$$\eta_{\mathrm{T}}(t)=\frac{h_5(t)-h_6(t)}{h_5(t)-h_{6,\mathrm{s}}(t)} \tag{17}$$

where $h_{6,s}$ is the enthalpy during isentropic expansion, which can be calculated by the equation of state,

$$h_{6,\mathrm{s}}(t)=f\left(s_{6,\mathrm{s}}(t),P_6(t)\right) \tag{18}$$

where P_6 is the outlet pressure of the turbine.

The entropies of the inlet and outlet of the turbine are the same during the isentropic expansion,

$$s_{6,\mathrm{s}}(t)=s_5(t) \tag{19}$$

For the transient modelling, the turbine isentropic efficiency is not constant owing to the changes of the inlet and outlet pressures. The efficiency is related to the expansion ratio, which is defined as the ratio of inlet to outlet pressures. Therefore, an empirical formula is chosen to characterize the relationship between the expansion ratio and the turbine isentropic efficiency [36, 46],

$$\eta_{\mathrm{T}}(t)=0.0269\left(\frac{P_5(t)}{P_6(t)}\right)+0.7501 \tag{20}$$

where P_5 and P_6 are the inlet and outlet pressures of the turbine, respectively.

3) High-pressure and low-pressure tanks

The high-pressure and low-pressure CO_2 storage tanks (HPT and LPT) operate in both charging and discharging, in which the dynamic calculation model is established based on the energy conservation equation [36],

$$\frac{d\left(m_{\mathrm{char}}u_{\mathrm{char}}\right)_{\mathrm{HPT}}}{dt}=\dot{m}_{\mathrm{char}}(t)h_3(t) \tag{21}$$

$$\frac{d\left(m_{\mathrm{dischar}}u_{\mathrm{dischar}}\right)_{\mathrm{HPT}}}{dt}=\dot{m}_{\mathrm{dischar}}(t)h_4(t) \tag{22}$$

$$\frac{d\left(m_{\mathrm{char}}u_{\mathrm{char}}\right)_{\mathrm{LPT}}}{dt}=\dot{m}_{\mathrm{char}}(t)h_1(t) \tag{23}$$

$$\frac{d\left(m_{\mathrm{dischar}}u_{\mathrm{dischar}}\right)_{\mathrm{LPT}}}{dt}=\dot{m}_{\mathrm{dischar}}(t)h_6(t) \tag{24}$$

where m is the mass of CO_2 in the tank, and u is the specific internal energy of CO_2.

4) Thermal energy storage device

The thermal energy storage (TES) device absorbs the heat of compression during the charging time and releases the heat to CO_2 fluid during the discharging time. The calculation of the heat exchange process for the working fluid is simplified as thermal equilibrium calculation with heat loss. The dynamic calculation model is,

$$Q_{\text{char}} = \int_{t_{\text{begin char}}}^{t_{\text{end char}}} \dot{q}_{\text{char}}(t)dt \tag{25}$$

$$Q_{\text{dischar}} = \int_{t_{\text{begin dischar}}}^{t_{\text{end dischar}}} \dot{q}_{\text{dischar}}(t)dt \tag{26}$$

$$Q_{\text{char}} = Q_{dischar} + Q_{loss} \tag{27}$$

$$\dot{q}_{\text{char}}(t) = \dot{m}_{\text{char}}(t)\left(h_2(t) - h_3(t)\right) \tag{28}$$

$$\dot{q}_{\text{dischar}}(t) = \dot{m}_{\text{dischar}}(t)\left(h_5(t) - h_4(t)\right) \tag{29}$$

where $\dot{q}$ and Q are the heat exchange at moment t and the total heat transfer capacity, respectively.

3.3 Model validation by experimental data

Since the experimental data about the compressed CO_2 energy storage system is not available in the existing literature, the validation is carried out in two aspects. First, as the CO_2 storage tank is the most typical and important dynamic component, and the experimental and simulation data can be found in [36, 37], the comparisons with available experimental and simulation results for low-pressure tank (LPT) pressure, high-pressure tank (HPT) pressure, and HPT temperature during the charging, and for LPT pressure and HPT pressure during the discharging are depicted in Fig. 5(a-e), respectively. Note that the difference between the simulation results and experimental data of temperature in HPT becomes large at the end of the curves in Fig. 5 (c). It is because the heat loss in the experiment cannot be ignored, while it is neglected in the simulations. As time and temperature increase, the simulation temperature is higher than the experimental one. But it can be observed that all the simulation results have a good agreement, which proves the accuracy of the modelling. In summary, an overall good agreement is observed for the dynamic model of the CO_2 storage tank.

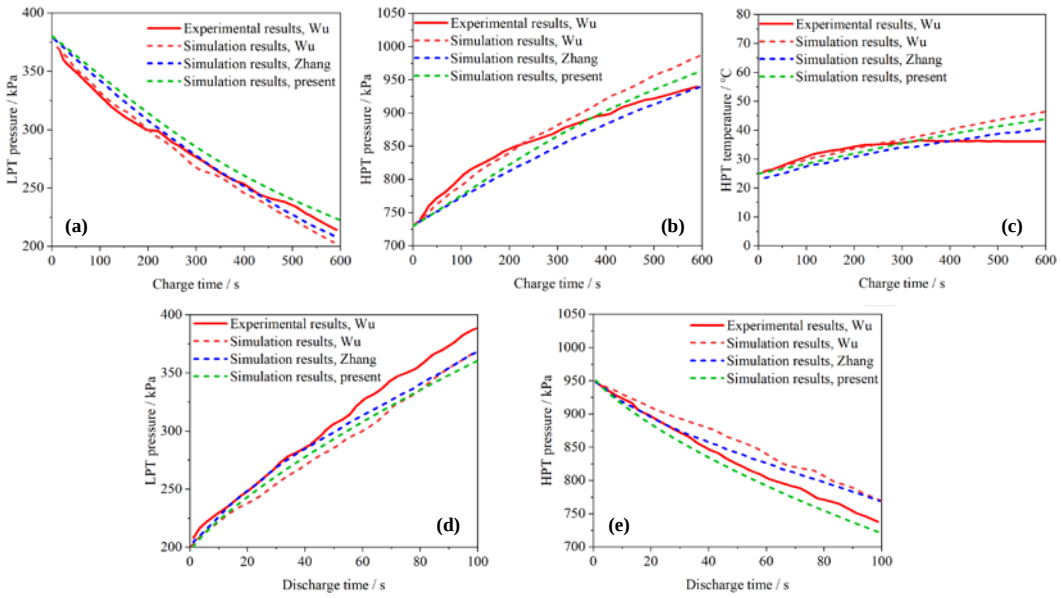

Fig. 5. Comparisons of the present results with available simulation and experimental data of (a) LPT pressure, (b) HPT pressure and (c) HPT temperature during charging; (d) LPT pressure and (e) HPT pressure during discharging [36, 37].

Second, as the dynamic modelling is also suitable for multi-stage energy storage systems after some simple modifications, the compressed CO_2 energy storage system with two-stage compression and two-stage expansion [36] is selected for the validation of the system. Fig. 6 illustrates the comparisons of the parameters of some key components. Good agreement is found for each component. Note that the TES modelling is different between the present results and the literature [36]: a slight difference occurs at the outlet of the TES device, resulting in the difference in the inlet parameters of the turbine, as well as the outlet parameters.

According to the validation on both component and system levels, the accuracy of the dynamic model can be verified.

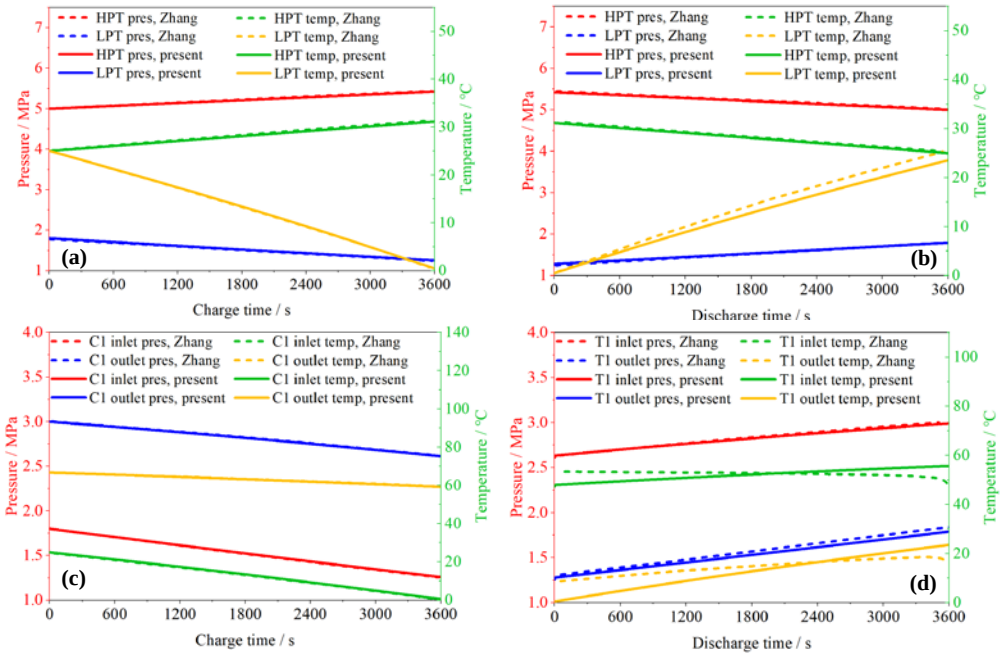

Fig. 6. Comparisons of (a) HPT/LPT pressure and temperature during the charging, (b) HPT/LPT pressure and temperature during the discharging, (c) C1 pressure and temperature during the charging, and (d) T1 pressure and temperature during the discharging [36].

4. Results

Overall, it is not straightforward to evaluate the comprehensive effects of the disturbances on the system performance. Thus, the analysis should begin from a simple scenario: only one single disturbance occurs, i.e., $p_{2nd} = P_{D,\,min}$ and p_{3rd} does not exist, and then turn to two other scenarios for more complex situations. In the second scenario, there are two disturbances, which are symmetric in the pressure curve, i.e., $p_{1st} = p_{3rd}$. In the third scenario, two asymmetric disturbances exist: p_{1st} is not equal to p_{3rd}. The three scenarios have different numbers of independent variables from one (p_{1st}), two (p_{1st} and p_{2nd}) to three (p_{1st}, p_{2nd} and p_{3rd}). The following sections investigate the effects of different numbers and the extent of the disturbances on system performance.

4.1 Effects of a single disturbance

The scenario with only one disturbance is analyzed here, as shown in Fig. 7(a), where the pressure at the high-pressure tank (HPT) in charging increases from $P_{D,\,min}$ until the pressure p_{1st}, and then turns to a discharging until the pressure at the HPT reaches $P_{D,\,min}$, marking the end of a round-trip. To evaluate the effects of the magnitude of p_{1st}, four typical cases are chosen in the scenario, where the

HPT is charged to 100%, 75%, 50% and 25% of its maximum charging capacity when the disturbance occurs, i.e., $p_{1st} = p_1$, $p_{0.75}$, $p_{0.5}$ and $p_{0.25}$. And the four typical cases are referred to as S1, S2, S3 and S4 ('S' for "single"), as schematic in Fig. 7(b), which is a rearrangement of the processes shown in Fig. 4.

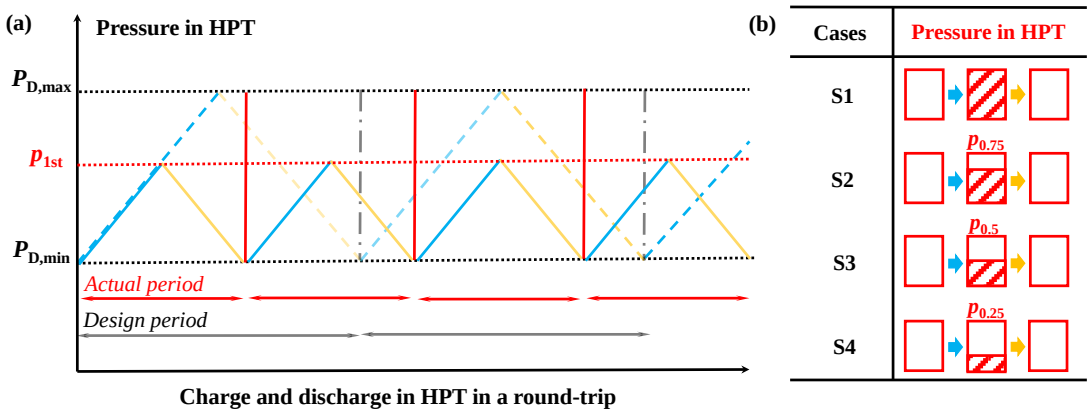

Fig. 7. Scenario of single disturbance (Scenario S): (a) there is only a single disturbance in a round-trip (the dashed lines denote design charging/discharging while the solid lines denote off-design ones); (b) schematic of the pressure changes in the HPT in the chosen four cases in this scenario.

The performances of the main components are investigated and presented in Fig. 8. As different components work during different periods, the temporal variations of the parameters of these components should be presented separately in different figures. The high-pressure tank (HPT) works during the charging and discharging processes, thus the parameters are shown in the two figures of "HPT charge" and "HPT discharge", as shown in Fig. 8 (a and b). For the low-pressure tank (LPT), the two figures are "LPT charge" and "LPT discharge", as shown in Fig. 8 (c and d). The parameters of the compressor are shown in the "Compressor charge" figures as it only works during the charging process, as shown in Fig. 8 (e and f). Thus, the turbine parameters are presented in "Turbine discharge" figures, as shown in Fig. 8 (g and h). For the thermal energy storage (TES) device, it works during both charging and discharging processes which require two figures of "TES charge" and "TES discharge", as shown in Fig. 8 (i and j).

The pressure and temperature in the HPT are presented in Fig. 8(a) and (b). With p_x in the HPT reduced from 100% to 25%, the charging time is reduced from 3632 s (t_0, actually the time at design condition) to 917 s (around $0.25t_0$). At the end of discharging the thermodynamic parameters of the HPT return to their initial values. Besides, the discharging time is the same as that in each case, and this is due to the assumptions of identical mass flow rates and the omission of valves. Additionally, the

variations of pressure and temperature in the LPT are depicted in Fig. 8(c) and (d). Note that the parameters at the end of discharging are different from the initial values. The reason should be that different heat loss values of the TES device during the discharging cause different turbine inlet parameters.

The isentropic efficiency of the compressor during charging is shown in Fig. 8(f). A disturbance occurring in the early stage, denoted in dashed orange, means that the compressor works mainly in the high-efficiency zone (compressor efficiency curve modelled by Eq. 14). Its isentropic efficiency decreases owing to enhanced outlet pressure and reduced inlet pressure. An enhanced power consumption observed should be due to an increase in the pressure difference of the compressor. The pressure and temperature differences increase with an increasing p_{1st} as given in Fig. 8(e), which are related to the increase of the pressure and temperature in the HPT and their decrease in the LPT during the charging.

The turbine isentropic efficiency during discharging is given in Fig. 8(h). For a certain case, it just decreases slightly when the disturbance occurs, as it still operates within design conditions. Among different cases, it decreases as the ratio of the outlet pressure and the inlet one is reduced, see Eq. 20. The turbine power output decreases owing to the pressure decrease in the HPT and the increase in the LPT. The pressure and temperature differences are given in Fig. 8(g). The initial pressure and temperature of the turbine in each case are different owing to the different parameters in the HPT when charging ends. Due to a similar cause to the compressor, the inlet and outlet parameters of the turbine both depend on those of the HPT and LPT. Therefore, the pressure and temperature differences in the turbine decrease with a decreasing p_{1st}, with the reduced pressure and temperature in the HPT and their increase in the LPT during the discharging.

TES device has a lower temperature when the disturbance occurs early as shown in Fig. 8(i) and (j). The temperature in the TES device is determined by the outlet temperature of the compressor, inlet temperature of the turbine and inlet/outlet temperature of the HPT, which has been analyzed above.

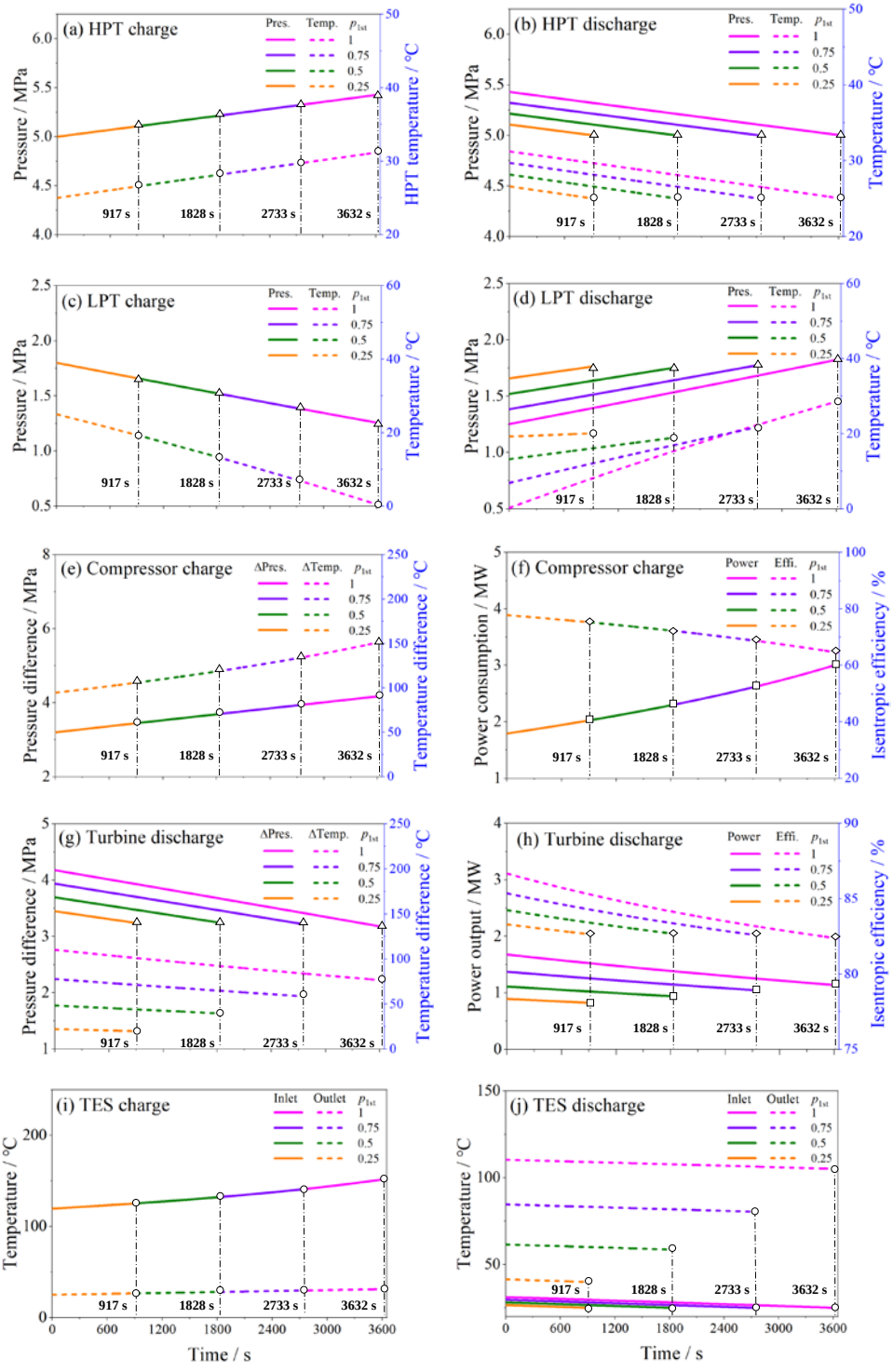

Fig. 8. Temporal variations of the parameters of main components: HPT pressure & temperature during charging (a) and discharging (b); LPT pressure & temperature during charging (c) and discharging (d); Compressor pressure & temperature difference (e) and power consumption & isentropic efficiency (f) during charging; Turbine pressure & temperature difference (g) and power consumption & isentropic efficiency (h) during discharging; TES temperature during charging (i) and discharging (j).

The exergy destruction (E_{Des}) and efficiency (η_{ex}) of the compressor, turbine and TES device are

shown in Fig. 9(a-c) based on Eqs. 4 and 8. With the rise of p_{1st}, an increasing E_{Des} is observed for the compressor because the fuel exergy is enhanced faster than the product exergy. Meanwhile, η_{ex} is only slightly reduced due to the small difference between the fuel and product exergy, meaning that there is little irreversibility in the compressor. For the turbine, E_{Des} is not monotonic because it is an absolute value of the difference between the fuel and product exergy, which is different at different p_{1st}. Nevertheless, η_{ex} increases linearly with the rise of p_{1st} as it is the ratio of the product to fuel exergy. The increasing η_{ex} illustrates more output power and less irreversibility in the turbine. Besides, η_{ex} of the TES device increases due to the faster growth of the product exergy than that of the fuel exergy. Tab. 2 shows the exergy calculation equations for each component.

Tab. 2. Exergy calculation equations for the compressor, turbine and TES device.

Components	Fuel exergy	Product exergy
Compressor	$\int_{t_{\text{begin char}}}^{t_{\text{end char}}} \dot{w}_{\text{C}}(t)dt$	$\int_{t_{\text{begin char}}}^{t_{\text{end char}}} \left(\dot{E}_{\text{C, out}}(t)-\dot{E}_{\text{C, in}}(t)\right)dt$
Turbine	$\int_{t_{\text{begin dischar}}}^{t_{\text{end dischar}}} \left(\dot{E}_{\text{T, in}}(t)-\dot{E}_{\text{T, out}}(t)\right)dt$	$\int_{t_{\text{begin dischar}}}^{t_{\text{end dischar}}} \dot{w}_{\text{T}}(t)dt$
TES device	$\int_{t_{\text{begin char}}}^{t_{\text{end char}}} \left(\dot{E}_{\text{TES, in}}(t)-\dot{E}_{\text{TES, out}}(t)\right)dt$	$\int_{t_{\text{begin dischar}}}^{t_{\text{end dischar}}} \left(\dot{E}_{\text{TES, out}}(t)-\dot{E}_{\text{TES, in}}(t)\right)dt$

At the system scale, the performance of the total and average output power (W_T and $\bar{W}_T$), energy storage density (ρ) and round-trip efficiency (η_{rt}), is shown in Fig. 9(d) and (e). The slope of W_T is greater than that of $\bar{W}_T$ as shown in Fig. 9(d). It is because W_T is the integral of the power over time as calculated in Eq. 16, in which a larger p_{1st} means a longer discharging time, resulting in a larger W_T. Meantime, $\bar{W}_T$ increases due to the increased exergy efficiency, which also contributes to higher total power output.

Furthermore, the effects of p_{1st} on η_{rt} and ρ are shown in Fig. 9(e) from Eqs. 2 and 3. ρ_D and $\eta_{rt,D}$ at design conditions (p_{1st} = 1) are 252.68 kJ·m^{-3} and 59.66%, respectively, marked by dashed lines for reference in Fig. 9(e). The blue bars are closer than the dashed blue line, while the white bars are farther than the dashed black line, indicating that the disturbance (p_{1st}) affects density more than efficiency. η_{rt} decreases to 44.95% with a decreasing p_{1st}, because of a reduction in the ratio of W_T to W_C (see Eq. 2). Moreover, ρ decreases to 39.29 kJ·m^{-3} (at p_{1st} = 0.25), which is 15.55% of ρ_D due to a reduced total power output.

The effect of p_{1st} on the system firstly depends on the turbine. As η_{ex} is down to the minimum

when p_{1st} decreases to 0.25 in Fig. 9(b), together with the minimum discharging time, W_T decreases to its smallest value which is about 15.55% of the design condition in Fig. 9(d). Note that the percentage is the same as the percentage ρ_D at p_{1st} = 0.25 in Fig. 9(e) according to Eq. 3, in which the volume of tanks is constant. In other words, W_T and ρ follow the same trend, which is shown by the white bars in Fig. 9(d) and (e).

However, in Fig. 9(e), the slope of η_{rt} is smaller owing to the combined effect of the turbine and the compressor according to Eq. 2. As there is little irrversibility caused by high η_{ex} on the compressor as shown in Fig. 9(a), the increase in η_{rt} is similar to that of the turbine, which is shown in Fig. 9(d) and (e). However, as η_{ex} of compressor decreases with the rise of p_{1st}, leading to an increase in the power comsumption, η_{rt} increases more slowly than the storage density which is affected only by the turbine. In summary, it is illustrated that when the disturbance occurs prematurely, a remarkable reduction will be inevitable in ρ, η_{rt}, W_T and $\bar{W}_T$.

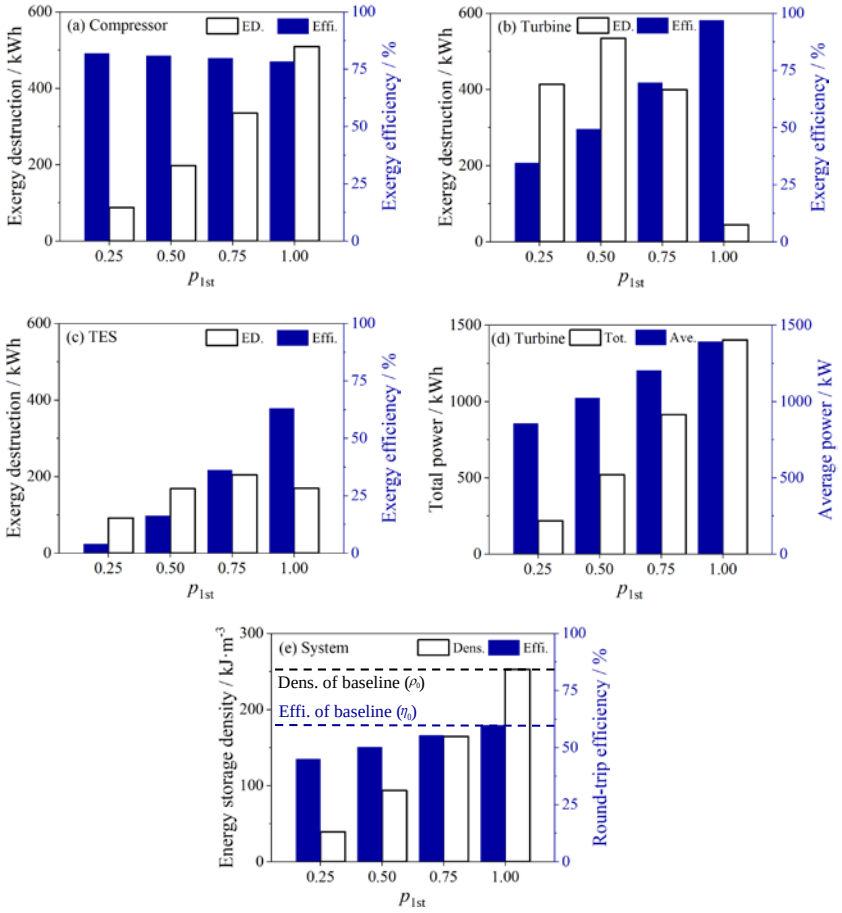

Fig. 9. Effects of single disturbance on the performance of components and the system: the exergy destruction and efficiency of (a) the compressor, (b) the turbine, (c) the TES device, (d) the total and average power of the turbine, and (e) the round-trip efficiency and energy storage density.

4.2 Effects of double symmetry disturbances

The second scenario is analyzed and evaluated based on two symmetric disturbances. As shown in Fig. 10(a), the pressure at the high-pressure tank (HPT) increases from $P_{D,\,min}$, stops at pressure p_{1st}, and then turns to discharging and stops at pressure p_{2nd}. After that, charging begins and then stops at the pressure p_{3rd} (= p_{1st}), followed by sufficient discharging. Six typical cases were chosen and referred to as DS1-6 ('DS' means double symmetric disturbances), as schematic in Fig. 10(b).

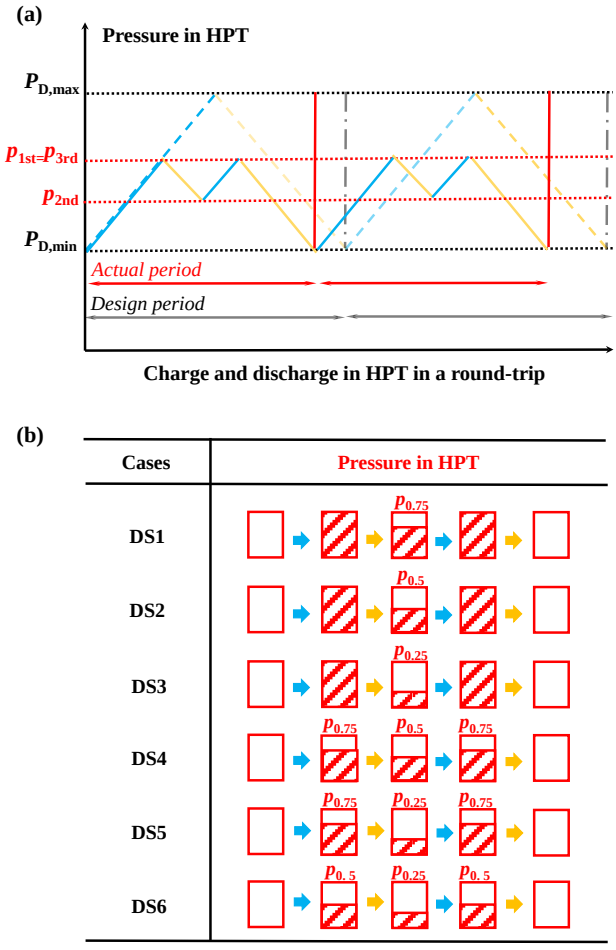

Fig. 10. Scenario of double symmetry disturbance (Scenario DS): (a) there are double disturbances in a round-trip, which are symmetrical with $p_{1st} = p_{3rd}$ (the dashed lines denote design charging/discharging while the solid denote off-design ones); (b) schematic of the pressure changes in the HPT in the chosen six cases in this scenario.

For a round-trip with multiple insufficient charging and discharging, the round-trip efficiency should be calculated in Eq. 30, where n is the number of discharging, $W_{T,\,k}$ is the total power output, and $W_{C,\,k}$ denotes the total power consumption in the k_{th} discharging. Similarly, the energy storage density in a round-trip is calculated in Eq. 31, where V denotes the volume of storage tank. Thus, the

exergy destruction is calculated in Eq. 32, where $\dot{E}_{\mathrm{D,i,\,n}}$, $\dot{E}_{\mathrm{F,i,\,n}}$ and $\dot{E}_{\mathrm{P,i,\,n}}$ represent the exergy destruction rate, the fuel exergy, and the product exergy rate in the i_{th} component, respectively. The exergy efficiency is calculated in Eq. 33.

$$\eta_{\mathrm{rt}} = \frac{\sum_{1}^{\mathrm{n}} W_{\mathrm{T,\,k}}}{\sum_{1}^{\mathrm{n}} W_{\mathrm{C,\,k}}} \tag{30}$$

$$\rho = \frac{\sum_{1}^{\mathrm{n}} W_{\mathrm{T,\,k}}}{nV} \tag{31}$$

$$\dot{E}_{\mathrm{Des,\,i}} = \frac{\sum_{1}^{\mathrm{n}} \dot{E}_{\mathrm{Des,\,i,\,k}}}{n} = \frac{\sum_{1}^{\mathrm{n}} \left(\dot{E}_{\mathrm{F,\,i,\,k}} - \dot{E}_{\mathrm{P,\,i,\,k}} \right)}{n} \tag{32}$$

$$\eta_{\mathrm{ex,\,i}} = \frac{\sum_{1}^{\mathrm{n}} E_{\mathrm{P,\,i,\,k}}}{\sum_{1}^{\mathrm{n}} E_{\mathrm{F,\,i,\,k}}} \tag{33}$$

The effects of two symmetric disturbances on the performance of the components and the system are demonstrated in Fig. 11. Note that the results in Fig. 8 are also added. The results on the exergy destruction and efficiency (E_{Des} and η_{ex}) of the compressor, turbine and TES device are shown in Fig. 11(a-c). For the cases with a certain $p_{2\mathrm{nd}}$, the results are similar to those in Scenarios S, as analyzed in Sec. 4.1. When $p_{1\mathrm{st}}$ is determined, as $p_{2\mathrm{nd}}$ increases, E_{Des} decreases, and η_{ex} increases in the compressor, turbine, and TES device. It is because $p_{2\mathrm{nd}}$ represents disturbance during the process. When $p_{2\mathrm{nd}}$ slightly deviates from 1, e.g., $p_{2\mathrm{nd}} = 0.75$, meaning a limited disturbance, so the main components still operate in their design conditions, leading to a limited E_{Des} and higher η_{ex}.

The total and average output power (W_{T} and $\bar{W}_{\mathrm{T}}$) of the turbine is shown in Fig. 11(d). According to Sec. 4.1, the variations of W_{T} and $\bar{W}_{\mathrm{T}}$ are dependent on η_{ex} of the turbine as shown in Fig. 11(d). Therefore, $\bar{W}_{\mathrm{T}}$ presents a similar trend to η_{ex}. However, W_{T} at $p_{2\mathrm{nd}} \neq 0$ is higher than that at $p_{2\mathrm{nd}} = 0$. It is because that W_{T} is the integral of the power at each moment during the whole process. The cases at $p_{2\mathrm{nd}} \neq 0$ present a longer actual period due to the disturbance which suffer from two charging/discharging in the process (compared to one charging/discharging at $p_{2\mathrm{nd}} = 0$).

W_{T} and $\bar{W}_{\mathrm{T}}$ of the turbine essentially determines η_{rt} and ρ of the system (see Sec. 4.1), which are shown in Fig. 11(e). In the dark-colored bars, the highest η_{rt} of 59.18% appears with $p_{1\mathrm{st}}$ =

1 and p_{2nd} = 0.25 (Case DS3), while the least one of 52.11% is observed with p_{1st} = 0.50 and p_{2nd} = 0.25 (Case DS6). This is also observed for the highest ρ of 224.35 kJ·m^{-3} (88.79% ρ_D) and the least one of 74.24 kJ·m^{-3} (29.38% ρ_D). It is not surprising to observe a slight difference in η_{rt}, but it is necessary to note the huge difference in ρ. The latter is caused by two reasons: 1) ρ depends on the extent of charging (p_{1st}); the insufficient charging no doubt undermines ρ. 2) It also depends on the extent of discharging (p_{3rd}); the insufficient discharging will also reduce ρ. Note that ρ can be reduced to less than 1/3 of ρ_D.

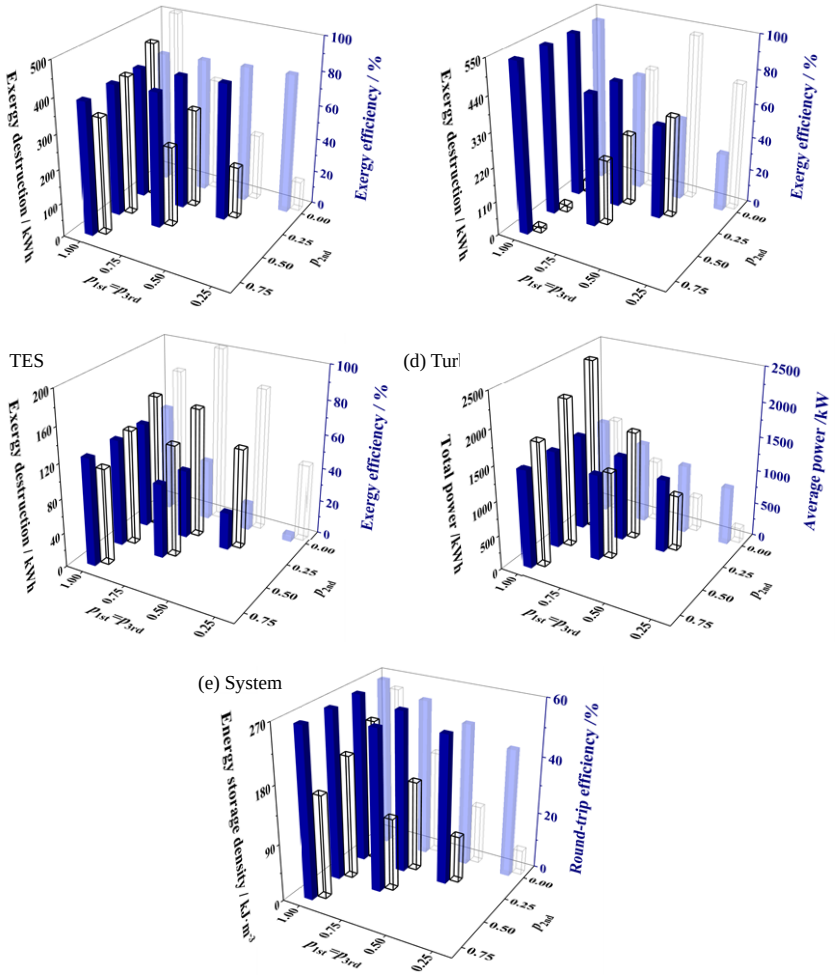

Fig. 11. Effects of two disturbances on the performance of the components and the system: the exergy destruction and efficiency of (a) the compressor, (b) the turbine, (c) the TES device, (d) the total and average power of the turbine, (e) the round-trip efficiency and energy storage density.

4.3 Effects of three different disturbances

The third scenario is analyzed and evaluated based on three different disturbances (p_{1st}, p_{2nd} and p_{3rd}) existing. As shown in Fig. 12(a), the pressure at the high-pressure tank (HPT) increases from $P_{D,}$

$_{min}$ and stops at p_{1st}, p_{2nd} and p_{3rd}, and then ends at $P_{D,\,min}$ again. Eight typical cases are chosen in the scenario, and referred to as DA1-8, as schematically shown in Fig. 12(b), where 'DA' means two asymmetric disturbances ($p_{1st} \neq p_{3rd}$).

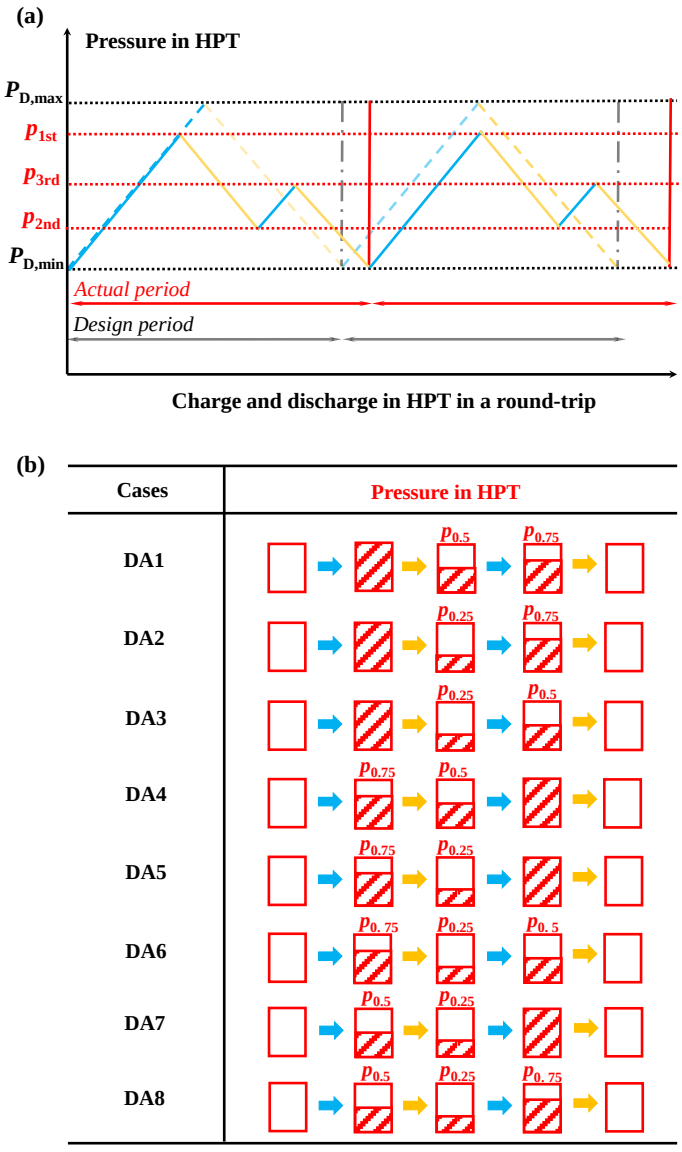

Fig. 12. Scenario of double asymmetry disturbance (Scenario DA): (a) there are double disturbances in a round-trip, which are asymmetrical with p_{1st} not equal to p_{3rd} (the dashed lines denote design charging/discharging while the solid denotes off-design ones); (b) schematic of the pressure changes in the HPT in the chosen eight cases in this scenario.

The effects of three different disturbances on the performance of the components and the system are demonstrated in Fig. 13. Note that the results of the cases in both Scenarios S and DS are added and marked by the ten spheres on the dashed triangle surface. The rest of the eight spheres in the space represent the cases for DA scenarios.

The maximum value of the total output power (W_T) is shown in blue circle in Fig. 13(a) due to the longest actual period as analyzed in Sec. 4.2. However, as the average output power ($\bar{W}_T$) is independent of time, the powers are all at a high level at $p_{1st} = p_{3rd} = 1$, as shown in Fig. 13(b). The energy storage density (ρ) is given in Fig. 12(c) while the round-trip efficiency (η_{rt}) is shown in Fig. 13(d). ρ is defined as the ratio of W_T and the number of charging/discharging in Eq. 31. The numbers of the charging/discharging are one at $p_{2nd} = 0$ and two at $p_{2nd} \neq 0$. Therefore, the maximum value is shown in red circle, which is also the position for the design condition. A larger ratio of W_T and W_C is observed when p_{3rd} rises, despite a close W_T. The third disturbance p_{3rd} has a more important effect on η_{rt}, and this is why we can observe a symmetric distribution of ρ in Fig. 13(c), rather than the efficiency in Fig. 13(d).

Moreover, we can observe that, among all the cases, ρ varies from 252.68 (ρ_D) to 39.29 kJ·m^{-3} (15.55% ρ_D). ρ in most cases has deviated significantly from that of the design condition (noted by the circle). However, η_{rt} varies from 59.66 ($\eta_{rt,D}$) to 44.95% (75.34% $\eta_{rt,D}$). Most of the cases present a slightly reduced η_{rt}. These findings also support the statements of Secs. 4.1 and 4.2. Thus, it can be concluded that, compared to η_{rt}, ρ suffers from a remarkable effect of multiple insufficient charging and discharging. This implies some issues for economic analysis, which will be discussed later.

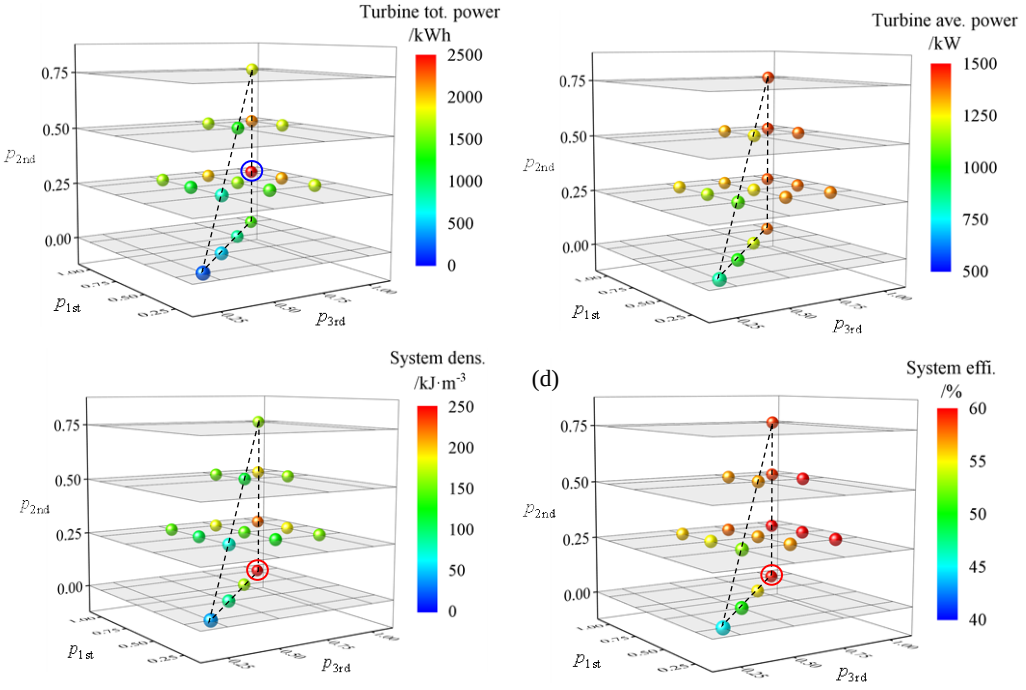

Fig. 13. Effects of three disturbances on the performance of the components and the system: (a) the

total and (b) the average power of the turbine, (c) the round-trip efficiency and (d) the energy storage density.

5 Discussion

The evaluations of the energy storage density, system efficiency and power output, under the effects of insufficient charging/discharging, are presented in Figs. 8, 10 and 12. The results demonstrate that the actual performance of density and power, except for the system efficiency, could highly deviate from the targets at design conditions. In other words, a perspective should be performed on the effects of renewable energy variability on comprehensive performance over a long period. It is assumed that the energy storage system would run half the design (S1 (p_0-p_{1st}-p_0) in single disturbance) and half the off-design (in which three single disturbances, six symmetrical double disturbances and eight asymmetrical double disturbances operate equally in quantity) processes. The actual comprehensive efficiency of the system under this assumption is 57.78%, slightly less than the design one of 59.66%. However, a remarkable reduction in energy storage density to 197.60 kJ·m^{-3} is observed, about 78.2% of the design value of 252.68 kJ·m^{-3}. Furthermore, the average output power of the turbine is about 95.70% of the design value.

Remarkable reductions in density and power should be considered seriously. If not well treated, it would bring some uncertainty and insecurity to larger-scale electricity grids. More importantly, this could fundamentally deteriorate the economic performance of an energy storage system over a long period. The effects of energy source variety on economic performance have been investigated in [47, 48], considering the effects of a variety of these parameters. However, the effects of insufficient charging and discharging, due to the variability of renewable energy have not been investigated before. The output power and the energy density evaluated in the present work could be incorporated with future work of techno-economic analysis. For example, He et al. [48] evaluated the geological resources of the UK for bulk-scale compressed air energy storage combined with solar and wind energy, in which the variability of solar energy (see Fig. 3 in [48]) through a year was considered in detail in calculating the output power (Eq. 10 in [48]). Considering the complex effects of the variability of renewables, improving the understanding of its effects will no doubt help the assessment of the economic cost and income under actual conditions over a long period.

Besides, it is noted that isobaric storage has drawn much attention owing to its potential to tackle

the transient pressure issue. For example, the Canadian company Hydrostor uses an isobaric design to reduce pressure loss for high-pressure air storage [49]. However, isobaric storage technologies, such as isobaric tanks with pistons or hydrostatic force, have huge complexity compared to the fixed-volume storage. The capital cost, configuration complexity, and other unpredictable challenges should be investigated. Especially for carbon dioxide storage, the isobaric tank would also face sealing issues, which is the key issue that should be considered.

6. Conclusions

In the present work, the effects of multiple insufficient charging and discharging on compressed CO_2 energy storage systems are proposed for the first time, mathematically formulated, and quantitatively evaluated. A novel analysis method is proposed. Firstly, the charging extent at high-pressure tank is chosen to define the insufficiency extent of charging and model the effects of external disturbance due to renewable energy uncertainty. Secondly, three typical scenarios are determined for showing the progressively higher dimension and a series of typical cases in each scenario are set. Thirdly, thermodynamic analysis is performed at different scales, from the temperature/pressure to the exergy analysis, the energy storage density, power output and system efficiency.

It is found that the actual efficiency of the system during the whole working period is 57.78%, slightly less than the design efficiency of 59.66%. However, the energy storage density is significantly reduced to 197.60 $kJ \cdot m^{-3}$, 78.2% of that at design conditions. Besides, the average output power of the turbine is about 95.70% of the design value. Note that there is still room for improvement in the present modelling, including more accurate modelling of the dynamic response of the components, specific modelling of the input of solar energy based on real geological resources conditions, and so on. Overall, the present work has demonstrated the important effects of renewable energy variability on the actual performance of energy storage systems and may help improve the accuracy of the economic analysis and facilitate the decarbonization of power systems.

CRediT authorship contribution statement

D L Yang: Conceptualization, Methodology, Data curation, Writing-original draft, review & editing. **G**

H Tang: Supervision, Funding acquisition, Resources, Writing-review & editing. **Q Sheng:** Methodology, Writing-review & editing. **X L Li:** Manuscript review. **Y H Fan:** Manuscript review. **Y L He:** Resources, Manuscript review. **K H Luo:** Supervision, Resources, Manuscript review.

Declaration of Competing Interest

The authors declare that they have no known competing financial interests or personal relationships that could have influenced the work reported in this paper.

Data availability

Data will be made available on request.

Acknowledgements

This work was supported by the National Natural Science Foundation of China under grant numbers of 51825604 and 51721004, and the 111 Project under grant number of B16038.

References

[1] Parag Y, Sovacool B. Electricity market design for the prosumer era. Nat Energy 2016; 1:16032.

[2] Ding Y, Li Y, Tong L, Wang L. Liquid air energy storage. Storing Energy 2022; 191-205.

[3] Vecchi A, Li Y, Ding Y, Mancarella, Sciacovelli A. Liquid air energy storage (LAES): A review on technology state-of-the-art, integration pathways and future perspectives. Adv Appl Energ 2021; 3:100047.

[4] Peng X, She X, Li C, Luo Y, Zhang T, Li Y, Ding Y. Liquid air energy storage flexibly coupled with LNG regasification for improving air liquefaction. Appl Energ 2019; 250:1190–201.

[5] Liu Z, Liu Z, Yang X, Zhai H, Yang X. Advanced exergy and exergoeconomic analysis of a novel liquid carbon dioxide energy storage system. Energ Convers Manag 2020; 205:112391.

[6] Chen H, Xu Y, Liu C, He F, Hu S. Storing energy in China—an overview. Storing Energy 2016; 509-527.

[7] Mileva A, Nelson J H, Johnston J, Kammen D M. SunShot solar power reduces costs and

uncertainty in future low-carbon electricity systems. Environ Sci Technol 2013; 47(16):9053–60.

[8] Lavine A S, Lovegrove K M, Jordan J, Anleu G B, Chen C, Aryafar H, Sepulveda A. Thermochemical energy storage with ammonia: Aiming for the sunshot cost target. AIP Conference Proceedings. AIP Publishing LLC 2016; 1734(1): 050028.

[9] Marion J, Kutin M, McClung A, Mortzheim J, Ames R. The STEP 10 MWe sCO_2 pilot plant demonstration. ASME Turbo Expo 2019: Turbomachinery Technical Conference and Exposition. American Society of Mechanical Engineers Digital Collection, 2019.

[10] Marion J, Lariviere B, Mcclung A, Mortzheim J, Ames R. The STEP 10 MWe S-CO_2 pilot demonstration status update. ASME Turbo Expo 2020: Turbomachinery Technical Conference and Exposition, 2020.

[11] SOLARSCO_2OL project. https://www.solarsCO_2ol.eu/the-project/.

[12] Le Moullec Y, Qi Z, Zhang J, Zhou P, Yang Z, Wang X, Chen W, Wang S. Shouhang-EDF 10MWe supercritical CO_2 cycle +CSP demonstration project. 3rd European Conference on Supercritical CO_2 (sCO_2) Power Systems 2019: 19th-20th September 2019. 2019: 138-147.

[13] Energy Dome. https://energydome.com/.

[14] Dongfang Electric Corporation. https://www.dongfang.com/.

[15] Wang M, Zhao P, Wu Y, Dai Y. Performance analysis of a novel energy storage system based on liquid carbon dioxide. Appl Therm Eng 2015; 91:812–23.

[16] Zhang Y, Yang K, Hong H, Zhong X, Xu J. Thermodynamic analysis of a novel energy storage system with carbon dioxide as working fluid. Renew Energy 2016; 99:682-697.

[17] Liu H, He Q, Borgia A, Pan Lehua, Oldenburg C. Thermodynamic analysis of a compressed carbon dioxide energy storage system using two saline aquifers at different depths as storage reservoirs. Energy Convers Manag 2016; 127:149-159.

[18] Zhang X, Wang G. Thermodynamic analysis of a novel energy storage system based on compressed CO_2 fluid. Int J Energ Res 2017; 41:1487–503.

[19] Yang D, Tang G, Luo K, Fan Y, Li X, Sheng Q. Integration and conversion of supercritical carbon dioxide coal-fired power cycle and high-efficiency energy storage cycle: Feasibility analysis based on a three-step strategy. Energ Convers Manag 2022; 269:116074.

[20] Mercangoz M, Hemrle J, Kaufmann L, Z'Graggen A, Ohler C. Electrothermal energy storage with transcritical CO_2 cycles. Energy 2012; 45:407-415.

[21] Liu J, Chen H, Xu Y, Wang L, Tan C. A solar energy storage and power generation system based on supercritical carbon dioxide. Renew Energy 2014; 64:43-51.

[22] Mecheri M, Le Moullec Y. Supercritical CO_2 Brayton cycles for coal-fired power plants. Energy 2016; 103:758-71.

[23] Le Moullec Y. Conceptual study of a high efficiency coal-fired power plant with CO_2 capture using a supercritical CO_2 Brayton cycle. Energy 2013; 49:32-46.

[24] Xu J, Sun E, Li M, Liu H, Zhu B. Key issues and solution strategies for supercritical carbon dioxide coal fired power plant. Energy 2018; 157:227-46.

[25] Fan Y, Yang D, Tang G, Sheng Q, Li X. Design of S-CO_2 coal-fired power system based on the multiscale analysis platform. Energy 2022; 240:122482.

[26] Yang D, Tang G, Li X, Fan Y. Capacity-dependent configurations of S–CO_2 coal-fired boiler by overall analysis with a unified model. Energy 2022; 245: 123246.

[27] Wang K, He Y L, Zhu H. Integration between supercritical CO_2 Brayton cycles and molten salt solar power towers: A review and a comprehensive comparison of different cycle layouts. Appl Energ 2017; 195:819-836.

[28] Guo J, Li M, He Y, Jiang T, Ma T, Xu J, Cao F. A systematic review of supercritical carbon dioxide(S-CO_2) power cycle for energy industries: Technologies, key issues, and potential prospects. Energ Convers Manag 2022; 258:115437.

[29] Fan Y, Tang G, Li X, Yang D. General and unique issues at multiple scales for supercritical carbon dioxide power system: A review on recent advances. Energy Conversion and Management 2022; 268:115993.

[30] Chai L, Tassou S. A review of printed circuit heat exchangers for helium and supercritical CO_2 Brayton cycles. Therm Sci Eng Prog 2020; 18:100543.

[31] Yang D, Tang G, Fan Y, Li X, Wang S. Arrangement and three-dimensional analysis of cooling wall in 1000 MW S–CO_2 coal-fired boiler. Energy 2020; 197:117168.

[32] Li X, Tang G, Fan Y, Yang D. A performance recovery coefficient for thermal-hydraulic evaluation of recuperator in supercritical carbon dioxide Brayton cycle. Energy Conversion and Management 2022; 256:115393.

[33] Nie B, Chen J, Du Z, Li Y, Zhang T, Cong L, Zou B, Ding Y. Thermal performance enhancement of a phase change material (PCM) based portable box for cold chain applications. J Energy

Storage 2021; 40: 102707.

[34] Tambunan H, Mare A, Pramana P, Harsono B, Syamsuddin A, Sriyono, Purnomoadi A, Prahastono I. A preliminary study of solar variability characteristic in single area for solar photovoltaic applications. Int J Electrical Engineering and Informatics 2021; 13:3.

[35] Zhao P, Xu W, Zhang S, Gou F, Wang J, Dai Y. Components design and performance analysis of a novel compressed carbon dioxide energy storage system: a pathway towards realizability. Energ Convers Manag 2021; 229:113679.

[36] Zhang Y, Wu Y, Yang K. Dynamic characteristics of a two-stage compression and two-stage expansion Compressed Carbon dioxide energy storage system under sliding pressure operation. Energ Convers Manag 2022; 254:115218.

[37] Wu SC. System analysis and experimental verification of compressed CO_2 energy storage. Tianjin: Tianjin University of Commerce; 2019.

[38] Sciacovelli A, Li Y, Chen H, Wu Y, Wang J, Garvey S, Ding Y. Dynamic simulation of Adiabatic Compressed Air Energy Storage (A-CAES) plant with integrated thermal storage – Link between components performance and plant performance. Appl Energ 2017; 185:16-28.

[39] Briola S, Marco P, Gabbrielli R, Riccardi J. A novel mathematical model for the performance assessment of diabatic compressed air energy storage systems including the turbomachinery characteristic curves. Appl Energ 2016; 178:758-772.

[40] Hartmann N, Vöhringer O, Kruck C, Eltrop L. Simulation and analysis of different adiabatic Compressed Air Energy Storage plant configurations. Appl Energ 2012; 93:541-548.

[41] Wan X, Wang K, Zhang C, Zhang T, Min C. Off-design optimization for solar power plant coupling with a recompression supercritical CO_2 Brayton cycle and a turbine-driven main compressor. Appl Therm Eng 2022; 209:118281.

[42] Thanganadar D, Fornarelli F, Camporeale S, Asfand F, Patchigolla K. Off-design and annual performance analysis of supercritical carbon dioxide cycle with thermal storage for CSP application. Appl Energ 2021; 282: 116200.

[43] Wang J, Wang J, Dai Y, Zhao P. Assessment of off-design performance of a Kalina cycle driven by low-grade heat source. Energy 2017; 138:459-472.

[44] Li H, Hu D, Wang M, Dai Y. Off-design performance analysis of Kalina cycle for low temperature geothermal source. Appl Therm Eng 2016; 107:728-737.

[45] Qin X, Liu H, Meng X, Wei X, Zhao L, Yang L. A study on the compressor frequency and optimal discharging pressure of the transcritical CO_2 heat pump system. Int J Refrig 2019; 99:101–13.

[46] Kim HJ, Ahn JM, Cho SO, Cho KR. Numerical simulation on scroll expander–compressor unit for CO_2 trans-critical cycles. Appl Therm Eng 2008; 28:1654–61.

[47] Zhang H, Wang L, Lin X, Chen H. Technical and economic analysis of Brayton-cycle-based pumped thermal electricity storage systems with direct and indirect thermal energy storage. Energy 2022; 239:121966.

[48] He W, Dooner M, King M, Li D, Guo S, Wang J. Techno-economic analysis of bulk-scale compressed air energy storage in power system decarbonisation. Appl Energ 2021; 282:116097.

[49] Hydrostor https://www.hydrostor.ca/